microRNA-590-3p regulates inflammation and organ dysfunction in sepsis mouse model via the Syap1-mediated TGF-β/Smad signaling pathway

Yiming Li (Yiming_dr2019@163.com)
First Affiliated Hospital of Fujian Medical University https://orcid.org/0000-0003-0676-2076
Yanjing Huang
First Affiliated Hospital of Fujian Medical University
Zhihong Lin
First Affiliated Hospital of Fujian Medical University
Xiaofeng Huang
First Affiliated Hospital of Fujian Medical University

Research

Keywords: Sepsis, microRNA-590-3p, Synapse-associated protein 1, Transforming growth factor beta/Smad signaling pathway, Inflammation, Organ dysfunction

Posted Date: November 2nd, 2021

DOI: https://doi.org/10.21203/rs.3.rs-1010677/v1

Abstract

Sepsis is a common cause of death among patients in intensive care unit. Recent evidence indicates that microRNAs (miRs) might serve as potential biomarkers facilitating an early diagnosis of sepsis. Herein, we aimed to examine the mechanisms by which miR-590-3p may regulate inflammatory response and organ dysfunction during sepsis progression. The Gene Expression Omnibus (GEO) database was used to identify differentially expressed genes in an established sepsis mouse model, and the related miRNAs and downstream regulatory pathways were predicted using web-available microarrays. A sepsis animal model was induced in mice by cecal ligation and puncture (CLP). Indices of cardiac function, serum myocardial enzymes, and organ function were measured to confirm successful generation of the sepsis mouse model. Cell apoptosis and inflammatory cytokine levels in lung and liver tissues were observed by TUNEL staining and ELISA. Furthermore, the interaction between miR-590-3p and Synapse-associated protein 1 (*Syap1*) was identified by dual luciferase reporter gene assay. The effect of miR-590-3p on inflammation and organ dysfunction was examined using gain- and loss-of-function experiments. *Syap1* was found poorly expressed, whereas miR-590-3p was highly expressed in the sepsis-affected mice. Moreover, the elevation of miR-590-3p markedly downregulated the expression of anti-inflammatory cytokines IL10, *Syap1*, TGF-β, Smad3, and NF-κB p65 in modeled mice. Indices of cardiac and organ function were decreased, serum myocardial enzyme indices were notably increased, and cell apoptosis and pro-inflammatory cytokines of lung and liver tissues were increased in modeled mice. Together these results demonstrated that miR-590-3p can block the TGF-β/Smad signaling pathway through downregulation of *Syap1* and, thereby, contribute to sepsis inflammation and organ dysfunction.

Introduction

Sepsis is a life-threatening severe disease resulting from an aberrant host response to bacterial infection and activation of the coagulation cascade. It can activate the human contact system, which serves as the inflammatory response mechanism targeting foreign surfaces, proteins, and pathogens (Kohler et al., 2019). Multiple organ dysfunction induced by severe sepsis can lead to chronic critical illness, featured in severe immune dysfunction and catabolism (Gotts and Matthay, 2016). Therefore, sepsis refers more specifically to severe diseases characterized by organ dysfunction instead of a general term for infection and its resultant systemic inflammatory response (Fernando et al., 2018). Although much recent progress has been made in understanding the pathophysiology of sepsis, its predictable management and modulation of the host immune response involved in sepsis remains a challenge (van der Poll et al., 2017). In this regard, improved understanding of the molecular underpinnings of the regulatory mechanisms implicated in inflammatory response and organ dysfunction in sepsis is imperative.

Transforming growth factor-β (TGF-β) superfamily signaling plays an important role in many cellular responses, such as cell proliferation and differentiation (Wrighton et al., 2009). A previous study has demonstrated that TGF-β1 is upregulated in the acute respiratory distress syndrome induced by sepsis (de Pablo et al., 2012). Synapse-associated protein 1 (*Syap1*) is a member of the synapse associated BSD domain protein family, and its immunoreactivity is widely distributed in the mouse brain (Schmitt et

al., 2016). Based on bioinformatic prediction, it might be possible that *Syap1* can mediate the TGF-β/Smad signaling pathway and thus affect inflammatory response and organ dysfunction in sepsis.

MicroRNAs (miRs), a class of non-coding RNA molecules, play important roles in cell differentiation, proliferation, and survival (Rupaimoole and Slack, 2017). MiR expression has been found altered in the course of several pathologic conditions, including inflammation, infection, and sepsis (Benz et al., 2016). MiRs have also been suggested as optimal biomarkers for improving the diagnosis of sepsis and for identifying various stages, which could in turn enable more prompt and effective treatment (Kingsley and Bhat, 2017). Furthermore, a prior study has demonstrated that miR-30a can suppress the liver cell proliferation and promote apoptosis *via* the JAK/STAT signaling pathway through modulating SOCS-1 expression in rats with sepsis (Yuan et al., 2019). Another study also verified that miR-494-3P could act as a regulator to alleviate inflammatory response in sepsis *via* targeting TLR6 (Wang et al., 2019). *In silico* screening using microRNA, RAID2.0 and TargetScan databases indicated that *Syap1* might be a target gene of miR-590-3p. Based on the existing evidence and our preliminary findings, we hypothesized that miR-590-3p may regulate the development of sepsis *via Syap1*-mediated TGF-β/*Smad* signaling pathway.

Materials And Methods

Ethics statement

The animal experiments were performed in strict accordance with the recommendations in the ‘Guide to the Management and Use of Laboratory Animals’ issued by the National Institutes of Health. The protocol for animal experiments was approved by the Institutional Animal Care and Use Committee of The First Affiliated Hospital of Fujian Medical University.

Microarray-based analysis

The TGF-β/Smad signaling pathway related genes were extracted from Malacards. A mouse sepsis related gene microarray dataset GSE9667 was downloaded from GPL339 ([MOE430A] Affymetrix Mouse Expression 430A Array) from the Gene Expression Omnibus (GEO) database (https://www.ncbi.nlm.nih.gov/gds/?Term=). Differential expression analysis of the gene-expression datasets was performed using the ‘limma’ package (http://www.bioconductor.org/packages/release/bioc/html/limma.html) in the R statistical environment ($|logFC|>2.0$, $p < 0.01$) and gene expression thermograms were drawn accordingly. Protein-protein interaction (PPI) analysis was performed to identify the relationships between key genes and pathways. Thereafter, the downstream regulatory pathways of the selected genes were identified through literature reviewing of previous studies. MicroRNA database (http://www.microrna.org/microrna/home.do), Redundant Arrays of Inexpensive Disks (RAID) 2.0 (http://www.rna-society.org/raid2/), and TargetScan database (http://www.targetscan.org/mmu_71/) were used to predict upstream miRs of the selected genes. Finally, intersecting results were identified by a Venn map to screen and determine most relevant upstream miRs.

Construction of a CLP-induced sepsis mouse model

A total of 70 BALB/c mice of specific pathogen free (SPF) grade (aged 6 - 8 weeks, weighing 20 - 25 g, purchased from Hunan SJA Laboratory Animal Co., Ltd., Hunan, China), were selected. The mice were acclimated for 1 week in a circadian rhythm environment at (24 ± 2)°C, with free access to water and food. Then 60 mice were randomly selected for construction of the CLP mouse model. In brief, these mice were anesthetized by intraperitoneal injection with pentobarbital (50 mg/kg). After anesthesia, a longitudinal incision of about 1 cm was made along the midline of the abdomen. The cecum was exposed with sterile tweezers, ligated at about 1 cm from the end, and punctured vertically with a 27G needle. The cecum was then returned to the abdominal cavity and the abdominal cavity was sutured layer by layer. Next, the mice were subcutaneously injected with preheated normal saline (1 mL) and rested until revival. Blood from the inferior vena cava was collected at 4 h, 12 h, and 24 h after operation, with the supernatant tested using the EDS-99 bacterial endotoxin test system. Mortality rate was observed at 12 h, 24 h, and 36 h after operation. Besides, white blood cell (WBC) in peripheral blood collected from the caudal vein was assayed under an optical microscope. If the mortality, endotoxin level, and WBC level of the CLP modeled mice were found higher than those of normal mice (health mice without any treatment), the mouse model was considered as successfully constructed. For CLP model verification, the successfully modeled mice were subcutaneously injected with normal saline or ceftriaxone (100 mg/kg). And 18 h after injection, the levels of inflammatory factors in plasma were observed. If after ceftriaxone treatment, the levels of inflammatory factors in plasma were significantly lower than that in mice treated with normal saline, the model was successfully established (Azeh et al., 2002;Patel et al., 2018). Totally, 52 mice were successfully modeled, with a successful model rate of 86.7% (Supplementary Figure 1).

Animal grouping and treatment

Eight healthy mice were selected as the normal control (health mice without any treatment). And 40 successfully modeled mice were selected and every 8 mice were injected via tail vein with miR-590-3p agomir (10 mg/kg, 200 μL), miR-590-3p antagomir (10 mg/kg, 200 μL miR-590-3p interference plasmid), *Syap1* interference lentivirus (specific interference with *Syap1* lentivirus), miR-590-3p agomir combined with *Syap1* interference lentivirus (10 mg/kg, 200 μL miR-590-3p agomir + *Syap1*), and the corresponding negative control (NC, CLP mouse injected via tail vein with equal volume sterile PBS). All agomir and antimiomir used above were ordered from Shanghai GenePharma Co., Ltd., (Shanghai, China). And 8 successfully modeled mice were selected as the blank control (The CLP mouse model without any treatment). After 12 h of treatment, the mice were anesthetized with ketamine and the thoracic cavity was opened. The lung tissues and liver specimens of the mice were collected and stored at -70°C for further examination.

Quantification of bacteria

Mice were euthanized on different days post-infection by cervical dislocation. Different organs were removed aseptically and homogenized in 1 mL normal saline. Serial dilutions of the homogenized tissues

were made and plated on nutrient agar plates. Plates were incubated at 37°C for 24 h and then bacterial counts were determined.

Biochemical indicator detection

Subsequently, 9 h after operation, the mouse heart function indicators were detected by aortic cannulation: mean arterial pressure (MAP), left ventricular systolic pressure (LVSP), and maximum rate of change of left ventricular pressure (+dp/dtma, -dp/dtmax) using MRBP (Shanghai Yuyan Instruments Co., Ltd., Shanghai, China). In addition, the myocardial enzymes aspartate aminotransferase (AST), alkaline phosphatase (AKP), lactate dehydrogenase (LDH), LDH-1, hydroxybutyrate dehydrogenase (α-HBDH), creatine kinase (CK), and creatine kinase isoenzyme (CKMB) index values in serum were measured.

Furthermore, 72 h after operation, the content of diamine oxidase (DAO) in the intestinal tissues was assessed. In addition, heparin anticoagulant arterial blood was collected and arterial oxygen partial pressure (PaO_2) was measured with a blood gas analyzer. Concentration of AST and alamine aminotransferase (ALT) in serum was also determined. After the mice were euthanized, the whole lungs were wet-weighed and then dried at 70°C for 24 h. Thereafter the dry weight of the whole lung was determined. The water content of the lung tissues was computed as the ratio of lung wet weight to dry weight (W/D).

Hematoxylin-eosin (HE) staining

Separate the lungs and livers of mice and put them in a pre-prepared fixative (10% formalin, Bouin's fixative) and fix them for 24 h. Perform regular gradient alcohol (concentrations of 70%, 80%, 90%,95%, 100%, respectively) on the lung tissues. After routine dehydration for 1 min, xylene transparent 2 times, 5 min/time, wax immersion and paraffin embedding, serial sectioning (5 μm) after wax block trimming, tissue sections were placed in an oven at 80°C for 1 h. Thereafter, the slices were stained with hematoxylin (No. H8070, Beijing Solarbio Science & Technology Co. Ltd., Beijing, China), and differentiated using acid water and ammonia water for 10 s each. Next, the sections were blued in ammonia water for 10 min, stained for another 2 min in eosin solution (PT001, Shanghai Bogoo Biotechnology Co., Ltd., Shanghai, China), dehydrated with gradient alcohol (1 min/each), transparentized with xylene for 2 times (1 min/each), and mounted. The histopathological changes in lungs and livers were then observed under an optical microscope (model DMM-300D, Shanghai Caikon Optical Instrument Co., Ltd., Shanghai, China).

TUNEL staining

The apoptosis of the lung and liver cells was assayed using TUNEL kit (Changsha Baijia Biological Technology Co., Ltd., Changsha, China). Paraffin slices were dewaxed by xylene, rehydrated with conventional gradient alcohol, and immersed in 3% H_2O_2 solution for 10 min at room temperature. Then, the sections were added with 50 μL of 20 μg/mL proteinase K (P6556, Sigma-Aldrich, Shanghai, China), and hydrolyzed at room temperature for 20 min to remove the tissue proteins. Citrate was added for antigen retrieval treatment for 30 min. Then, 50 μL of Terminal deoxynucleotidyl transferase (TdT)

enzyme reaction solution was added and the sections were placed in a wet box in dark conditions at 37°C for 1 h. A TdT enzyme-free reaction solution was used for treating the negative control group. Thereafter, 4',6-diamidino-2-phenylindole solution (C1002, Beyotime Biotechnology, Co., Ltd., Shanghai, China) was added and developed for 10 min at room temperature. After being sealed with neutral resin, the sections were observed and photographed under a fluorescence microscope (BX53, Olympus, Tokyo, Japan). The positive cells were stained blue. A total of 10 visual fields were randomly selected and the ratio of positive cells to total cells was counted as apoptosis index (AI).

Enzyme linked immunosorbent assay (ELISA)

The known antigen was diluted to 1-10 μg/mL with carbonate-coated buffer (pH 9.6). Each well was added with 0.1 mL antigen and placed overnight at 4°C. Each well was then added with 0.1 mL of diluted supernatant and incubated at 37°C for 1 h. Blank, negative, and positive controls were prepared. The wells were added with 0.1 mL of freshly diluted enzyme-labeled secondary antibody (Abcam Inc., Cambridge, UK), incubated at 37°C for 35-60 min, and then washed with ddH_2O. Then, tetramethylbenzidine substrate solution (0.1 mL) was added to each well, incubated at 37°C for 10-30 min, and 50 mL of termination solution was added to terminate the color development. Thereafter, the optical density (OD) of each well was measured at a 450 nm wavelength within 20 min. Finally, the concentrations of tumor necrosis factor-α (TNF-α), interleukin (IL)-1β, IL-6, IL-10, and interferon (IFN)-γ (Wuhan Merck Biotechnology Co., Ltd., Wuhan, China) were calculated according to the regression equation of the standard curve. The above data processing was conducted through the calculation of tissue weight, and the concentration was compared with the tissue weight to obtain the amount of inflammatory factors in each g tissue as the evaluation standard.

Dual-luciferase reporter assay

The gene fragment of artificially synthesized *Syap1* untranslated region (3'-UTR) was introduced into a pMIR-reporter (Beijing Huayueyang Biotechnology Co., Ltd., Beijing, China) by using endonuclease sites Spel and Hind III. Next, a complementary sequence mutation site of seed sequence was designed and the target fragments were inserted into pMIR-reporter plasmid by T4 DNA ligase after restriction endonuclease cleavage. The correctly sequenced luciferase reporter plasmids WT and mutant (MUT) were co-transfected with miR-590-3p mimic into the HEK-293T cells respectively. After 48 h of transfection, cells were harvested and lysed, and their luciferase activities were assessed using a luciferase assay kit.

Cell culture and plasmid transfection

Lung epithelial cells A549 were transfected with different contents of *Syap1* plasmid, and Western blot was used to detect Smad phosphorylation and expression of inflammatory factors. The cells were further treated with TGF-β/Smad signaling pathway inhibitor LDN-193189 for 36 h after transfection and waited for 8 h. Western blot was used to detect Smad phosphorylation and expression of inflammatory factors. And we used LDN-193189 (inhibitor of BMP signaling pathway) to abolish the effect of *Syap1* on TGF-

β/Smad signaling pathway to analyze and compare the correlation between *Syap1* and TGF-β/Smad signaling pathway.

Lung epithelial cell A549 was transfected with different contents of *Syap1* plasmid and Western blot was used to determine the Smad phosphorylation and expression of inflammatory factors. A549 was further treated with the TGF-β/Smad signaling pathway inhibitor LDN-193189 for 36 h, and Western blot was used again to determine Smad phosphorylation and expression of inflammatory factors. It was observed that LDN-193189 reversed the promoting role of *Syap1* in the TGF-β/Smad signaling pathway and expression of inflammatory factors.

RNA isolation and quantification

Total RNA was extracted from lung tissues using a TRIzol kit (15596-026, Invitrogen, Gaithersburg, MD, USA). The RNA was reverse transcribed into cDNA strictly following the instructions of the reverse transcription kit (K1621, Fermentas, Maryland, NY, USA). The primer sequences were designed (Table 1), and submitted to GenScript Biotech Corp. (Nanjing, China) for synthesis. The mRNA expression of each gene was measured using a real-time PCR instrument (ABI 7500, ABI, Foster City, CA, USA) using the PCR kit (Takara, Dalian, China). β-actin was taken as an internal reference, and the relative expression of each gene was calculated by the $2^{-\Delta\Delta Ct}$ method.

Table 1
Primer sequences for qPCR

Targets	Primer sequences
miR-590-3p	F: GAGCTTATTCATAAAAGT-3'
	R: TCCACGACACGCACTGGATACGAC-3'
SYAP1	F: GGAATTTCCTCCGTGACCCA-3'
	R: CTTTCCAGAGGCTTGCTGCT-3'
TGF-β	F: CCACCTGCAAGACCATCGAC-3'
	R: CTGGCGAGCCTTAGTTTGGAC-3'
smad3	F: AGGGGCTCCCTCACGTTATC-3'
	R: CATGGCCCGTAATTCATGGTG-3'
NF-κB p65	F: ATGGCAGACGATGATCCCTAC-3'
	R: CGGAATCGAAATCCCCTCTGTT-3'
TNF-α	F: CAGGCGGTGCCTATGTCTC-3'
	R: CGATCACCCCGAAGTTCAGTAG-3'
IL-1β	F: GAAATGCCACCTTTTGACAGTG-3'
	R: TGGATGCTCTCATCAGGACAG-3'
IL-6	F: CTGCAAGAGACTTCCATCCAG-3'
	R: AGTGGTATAGACAGGTCTGTTGG-3'
β-actin	F: GTCGAGTCGCGTCCACC-3
	R: GTCATCCATGGCGAACTGGT-3"

Western blot

Lung tissue samples (50 mg) were added with protein lysate (R0010, Beijing Solarbio Science & Technology Co., Ltd.), and then homogenized at 3000 r/min until being fully lysed. After that, the mixture was bathed in ice for 30 min at 4℃, centrifugated at 12000 r/min for 15 min, and the supernatant was taken. The protein concentration of the supernatant was determined using a bicinchoninic acid (BCA) protein quantitation kit (23225, Pierce, Rockford, IL, USA), and adjusted to 1 μg/μL. Next, 20 μg of protein was loaded in each well for electrophoresis separation using 10% sodium dodecyl sulfate polyacrylamide gel electrophoresis (SDS-PAGE) gel (P1200, Beijing Solarbio Science & Technology Co. Ltd.,). The protein sample was then transferred to a polyvinylidene fluoride membrane (HVLP04700, Millipore, Bedford, MA, USA). The membrane was washed with tris-buffered saline tween (TBST) twice, and blocked with 5% skim milk solution for 2 h. The membrane was incubated with primary polyclonal antibodies: rabbit anti-

Syap1 (1 : 1000, ab175404), TGF-β (1 : 1000, ab9785), S*mad3* (1 : 1000, ab40854), NF-κB p65 (1 : 50000, ab32536), TNF-α (1 : 500, ab6671), IL-1β (1 : 1000, ab106035), or IL-6 (1 : 20, ab7737), overnight at 4°C. All antibodies were purchased from Abcam (Cambridge, UK). Then, the membrane was rinsed with TBST for 3 times (10 min/each), incubated with horseradish peroxidase (HRP)-labeled goat anti-rabbit immunoglobulin G (IgG) secondary antibody (1 : 2000, sc-2004, Santa Cruz Biotechnology, Inc, Santa Cruz, CA, USA) for 1 hour, and then developed using diaminobenzidine (DAB) liquid. Images were obtained using a gel imager (Gel Doc XR, Bio-Rad, Hercules, CA, USA), and the ratio of the gray value of the protein to that of the internal reference was considered as the relative expression of the protein with glycerlyceraldehyde-3-phosphate dehydrogenase (GAPDH) as the internal reference gene.

Statistical analysis

SPSS 21.0 (IBM Corp. Armonk, NY, USA) was used for statistical analysis. The measurement data was presented as mean ± standard deviation, and unpaired *t* test was used for comparison between two sets of data following normal distribution and homogeneity of variance. One-way analysis of variance (ANOVA) was used for the data comparisons between multiple groups, with Tukey's post hoc test. The difference was considered statistically significant when $p < 0.05$.

Results

miR-590-3p-Syap1-TGF-β/Smad signaling axis is involved in sepsis

A total of 94 genes related to TGF-β/Smad signaling pathway were extracted from Malacards, and 11 upregulated genes along with 58 downregulated genes were obtained from dataset GSE9667-GPL339 (Figure 1A), among which *Syap1* was found as poorly expressed in sepsis (Figure 1B). It has been found that *Syap1* is a very important downregulated gene in human hepatocellular carcinoma, and may serve as a potential key effector and recognition marker of this cancer, and *Syap1* is widely expressed in the central nervous system and has a regional specific distribution pattern (Chang et al., 2001; Schmitt et al., 2016).

Further, PPI analysis using the String database revealed that *Syap1* may indirectly regulate the TGF-β/Smad signaling pathway (Figure 1C). There were 58 upstream miRs of *Syap1* found in the database microRNAs, 97 in RAID 2.0, and 273 in TargetScan. The Venn diagram showed that there were four miRs (mmu-miR-291a-3P, mmu-miR-340-5p, mmu-miR-384-5p, and mmu-miR-590-3p) at the intersection of the results from these three databases (Figure 1D). Based on the above information, we speculated that miR-590-3p might modulate *Syap1* expression and further regulate the TGF-β/Smad signaling pathway to function in sepsis development.

Effects of miR-590-3p/ Syap1 axis **on cardiac function and serum myocardial enzyme assays**

Subsequently, mouse CLP model was established, and the modeled mice were injected via tail vein with miR-590-3p agomir, miR-590-3p antagomir, and *Syap1* interference lentivirus in combination or alone to identify their roles in sepsis. The cardiac function indices (Table 2) and serum myocardial enzyme indices (Table 3) of each group were measured 9 h after operation. The results showed that compared with the normal group, the MAP, LVSP, and AKP indicators of the other groups were significantly reduced, and the +dp/dtma, -dp/dtma, AST, LDH, LDH-1, α-HBDH, CK, and CKMB indicators were significantly increased ($p < 0.05$). There was no significant difference in mice treated with sterile PBS or co-treated with miR-590-3p agomir and *Syap1* in comparison with the blank control ($p > 0.05$). Moreover, compared with blank control, the expression of MAP ($p < 0.0001$), LVSP ($p = 0.002$), and AKP ($p = 0.033$) was remarkably decreased, while the +dp/dtma ($p < 0.0001$), -dp/dtma ($p < 0.0001$), AST ($p < 0.0001$), LDH ($p < 0.0001$), LDH-1 ($p < 0.0001$), α-HBDH ($p < 0.0001$), CK ($p < 0.0001$), and CKMB ($p < 0.0001$) indices was increased in the modeled mice injected with the miR-590-3p agomir. However, compared with blank control, the expression of MAP (miR-590-3p antagomir: $p < 0.0001$; *Syap1*: $p < 0.0001$), LVSP (miR-590-3p antagomir: $p < 0.0001$; *Syap1*: $p < 0.0001$), and AKP (miR-590-3p antagomir: $p < 0.0001$; *Syap1*: $p < 0.0001$) was remarkably increased, while the +dp/dtma (miR-590-3p antagomir: $p = 0.0002$; *Syap1*: $p = 0.002$), -dp/dtma (miR-590-3p antagomir: $p = 0.009$; *Syap1*: $p = 0.004$), AST (miR-590-3p antagomir: $p = 0.001$; *Syap1*: $p = 0.001$), LDH (miR-590-3p antagomir: $p < 0.0001$; *Syap1*: $p < 0.0001$), LDH-1 (miR-590-3p antagomir: $p = 0.001$; *Syap1*: $p = 0.002$), α-HBDH (miR-590-3p antagomir: $p = 0.001$; *Syap1*: $p = 0.001$), CK (miR-590-3p antagomir: $p < 0.0001$; *Syap1*: $p < 0.0001$), and CKMB (miR-590-3p antagomir: $p < 0.0001$; *Syap1*: $p < 0.0001$) indices was reduced in the mice infected with miR-590-3p antagomir or *Syap1*.

Table 2
The detection results of heart function index

Group	MAP (kPa)	LVSP (kPa)	+dp/dtmax (kPa/ms)	-dp/dtmax (kPa/ms)
Normal	15.88 ± 1.21	29.07 ± 3.04	143.65 ± 14.78	122.54 ± 12.86
Blank	4.02 ± 0.43*	12.44 ± 2.01*	285.73 ± 28.94*	244.76 ± 24.78*
NC	4.27 ± 0.51*	11.17 ± 1.22*	280.54 ± 27.96*	239.86 ± 23.56*
miR-590-3p agomir	2.04 ± 0.51*#	7.14 ± 1.02*#	533.89 ± 53.12*#	500.76 ± 50.83*#
miR-590-3p antagomir	8.18 ± 0.81*#	23.15 ± 3.44*#	210.67 ± 21.85*#	193.78 ± 19.45*#
SYAP1	8.44 ± 0.91*#	24.87 ± 3.43*#	221.76 ± 22.73*#	189.53 ± 18.94*#
miR-590-3p agomir+SYAP1	4.11 ± 0.51*	13.55 ± 2.22*	283.78 ± 28.56*	242.75 ± 24.74*

Table 3
The detection results of serum myocardial enzyme index (U/L, x ± s, n = 8)

Group	AST	AKP	LDH	LDH-1	α-HBDH	CK	CKMB
Normal	112.99 ± 12.01	151.81 ± 16.22	237.31 ± 59.03	244.71 ± 40.15	117.22± 20.34	402.86 ± 40.23	275.42 ± 80.76
Blank	225.98 ± 23.41*	57.22 ± 6.01*	938.14 ± 95.29*	448.23 ± 45.18*	237.18 ± 24.56*	701.34 ± 51.23*	941.23 ± 95.23*
NC	215.34 ± 22.56*	62.14 ± 7.12*	911.23 ± 94.97*	421.23 ± 44.56*	221.22 ± 35.14*	716.22 ± 54.56*	921.54 ± 93.21*
MIR-590-3p agomir	451.96 ± 46.23*#	40.15 ± 4.13*#	1876.34 ± 186.16*#	896.46 ± 90.23*#	474.36 ± 48.34*#	1200.68 ± 101.23*#	1832.45 ± 183.45*#
MIR-590-3p antagomir	161.23 ± 20.76*#	115.89 ± 13.23*#	469.18 ± 47.09*#	330.12 ± 40.16*#	167.22 ± 21.23*#	550.33 ± 46.98*#	532.18 ± 55.12*#
SYAP1	160.23 ± 43.78 *#	134.29 ± 14.01*#	531.18 ± 54.45*#	335.21 ± 42.44*#	170.34 ± 20.65*#	530.67 ± 44.89*#	604.56 ± 62.78*#
MIR-590-3P agomir+SYAP1	230.46 ± 20.23*	52.34 ± 6.21*	958.21 ± 99.22*	460.17 ± 50.45*	247.76 ± 29.01*	687.25 ± 50.87*	953.79 ± 96.23*

Effects of miR-590-3p/ Syap1 axis **on organ function of sepsis mice**

Compared with normal mice, the expression of DAO and PaO_2 in the modeled mice was reduced, while the expression of AST, ALT and W/D was significantly upregulated ($p < 0.05$). However, there was no significant difference in each index in the mice treated with sterile PBS or co-treated with miR-590-3p agomir and *Syap1* in comparison with the blank control ($p > 0.05$). Compared with the blank control, expression of DAO ($p < 0.0001$) and PaO_2 ($p = 0.0002$) was found significantly declined, and the expression of AST ($p < 0.0001$), ALT ($p < 0.0001$), and W/D ($p < 0.0001$) was significantly increased in the mice injected with miR-590-3p agomir. Compared with the blank control, expression of DAO (miR-590-3p antagomir: $p < 0.0001$; *Syap1*: $p < 0.0001$) and PaO_2 (miR-590-3p antagomir: $p < 0.0001$; *Syap1*: $p < 0.0001$) was found significantly enhanced, and the expression of AST (miR-590-3p antagomir: $p < 0.0001$; *Syap1*: $p < 0.0001$), ALT (miR-590-3p antagomir: $p = 0.031$; *Syap1*: $p = 0.037$), and W/D (miR-590-3p antagomir: $p < 0.0001$; *Syap1*: $p = 0.0001$) was significantly decreased in the mice injected with miR-590-3p antagomir or *Syap1* (Table 4).

Table 4
The detection results of mice organ function index

Group	DAO (ug/mL)	PaO_2 (kPa)	AST (u/L)	ALT (u/L)	W/D	Bacterial load (Log cfu/ml)
Normal	64.23 ± 7.12	31.04 ± 4.44	185.23 ± 12.56	36.22 ± 4.56	4.18 ± 0.61	3.82±3.02
Blank	31.08 ± 4.11*	11.08 ± 2.01*	279.11 ± 16.98*	60.22 ± 8.78*	13.98 ± 2.43*	4.44±3.59
NC	32.18 ± 4.24*	11.87 ± 2.45*	271.04 ± 17.01*	61.02 ± 7.41*	14.07 ± 1.69*	4.37±3.46
miR-590-3p agomir	14.28 ± 2.03*#	4.27 ± 0.44*#	329.44 ± 15.28*#	81.27 ± 8.23*#	21.24 ± 3.45*#	4.59±3.67
miR-590-3p antagomir	47.24 ± 5.23*#	19.22 ± 2.89*#	237.98 ± 14.67*#	48.98 ± 5.77*#	8.11 ± 0.92*#	4.11±3.32
SYAP1	44.92 ± 5.67*#	20.16 ± 3.45*#	239.27 ± 15.01*#	49.22 ± 5.78*#	8.97 ± 0.98*#	4.09±3.02
miR-590-3p agomir + SYAP1	29.08 ± 2.41*	10.22 ± 1.54*	274.18 ± 16.66*	62.48 ± 6.76*	14.56 ± 2.06*	4.47±3.66

Note: * $p < 0.05$ *vs.* normal mice; # $p < 0.05$ *vs.* the blank control and the NC. The data were all measurement data and expressed as mean ± standard deviation. One-way ANOVA was used for comparison among multiple groups, with Tukey's post hoc test, n = 8. DAO, diamine oxidase; AST, aspartate aminotransferase; ALT, alamine aminotransferase; W/D, wet weight/dry weight.

Effects of miR-590-3p/ Syap1 axis **on histopathological changes in sepsis mice**

HE staining results (Figure 2A-B) demonstrated that the normal mice had intact alveolar structure, normal alveolar septum without obvious edema fluid, red blood cells or inflammatory cells in the alveolar cavity. In addition, the liver tissue structure was clear, and the liver cells were arrayed neatly without much swelling and necrosis. The lung tissues of the modeled mice without any treatment and modeled mice treated with sterile PBS showed slight inflammatory infiltration and alveolar structure and interval, with swollen liver, partially necrotic cells as well as inflammatory cell infiltration in the portal area with marked proliferation of Kupffer cells in the sinusoids.

The mice injected with miR-590-3p agomir exhibited severe destruction of lung tissues structure, pulmonary hemorrhage, alveolar expansion, increased alveolar septum, thickened alveolar wall, and transparent membrane formation, accompanied by a large number of inflammatory cell infiltration and obvious edema in the lungs. In addition, massive necrosis of liver cells and pronounced infiltration of inflammatory cells were observed in the liver HE staining results of these mice. However, the degree of lung tissue damage in the mice injected with miR-590-3p antagomir and mice injected with *Syap1* was less severe than the modeled mice without any treatment and modeled mice treated with sterile PBS, which exhibited despite the pulmonary interstitial and alveolar septal congestion and edema, complete

alveolar cavity was clear with a small amount of edema and red blood cells in the lungs of these treated mice. Besides, there were fewer necrotic cells, and less proliferation of Kupffer cells in the livers of these treated mice. There was no significant difference in histopathological changes among the modeled mice without any treatment, modeled mice treated with sterile PBS, and those co-treated with miR-590-3p agomir and *Syap1*. These findings indicated that miR-590-3p contributed to more severe inflammation of liver and lung tissues in modeled mice.

miR-590-3p suppression or Syap1 upregulation impedes apoptosis of cells in lung and liver tissues of mice

TUNEL staining results (Figure 3) suggested that normal mice exhibited few positive cells with low apoptotic rate as apoptotic cells were stained brown in TUNEL staining. Compared with the normal mice, the apoptotic rate of lung tissues and liver tissues in the modeled mice was markedly higher ($p < 0.05$). Compared with modeled mice without any treatment and modeled mice treated with sterile PBS, the apoptotic rate of the lung tissues ($p < 0.0001$) and liver tissues ($p < 0.0001$) of the modeled mice injected with miR-590-3p agomir was dramatically increased, but apoptotic rate of the lung tissues ($p < 0.0001$) and liver tissues ($p < 0.0001$) strikingly reduced in the modeled mice injected with miR-590-3p antagomir or *Syap1*. There was no significant difference in apoptotic rate between the mice injected with miR-590-3p antagomir or SYAP1 ($p > 0.05$). Also, there was no significant difference in apoptotic rate of the modeled mice without any treatment, modeled mice treated with sterile PBS, and those co-treated with miR-590-3p agomir and *Syap1* ($p > 0.05$).

Inhibition of miR-590-3p alleviate inflammation response

According to the results of ELISA, levels of related inflammatory factors in serum, lung, and liver were consistent (Figure 4). Compared with the normal mice, levels of pro-inflammatory cytokines TNF-α, IL-1β, IL-6, and IFN-γ was increased, and the level of anti-inflammatory cytokine IL-10 was reduced in the serum, lung, and liver in the modeled mice ($p < 0.05$). In comparison with the blank control and the NC, levels of TNF-α, IL-1β, IL-6, and IFN-γ in the mice treated with miR-590-3p agomir were notably raised, but IL-10 level was significantly lower ($p < 0.05$), while it was opposite in mice treated with miR-590-3p antagomir or *Syap1* ($p < 0.05$). In addition, among the modeled mice without any treatment, modeled mice treated with sterile PBS, and those co-treated with miR-590-3p agomir and *Syap1*, the levels of related inflammatory factors had no significant differences ($p > 0.05$).

Syap1 is adversely targeted by miR-590-3p

A specific binding region between the *Syap1* gene sequence and the miR-590-3p sequence was predicted by Web-available microarrays indicating that *Syap1* might be a target gene of miR-590-3p, which was further verified by luciferase reporter assay (Figure 5A). The results displayed that compared with the NC, the luciferase activity of the WT-*Syap1* was dramatically reduced in the miR-590-3p transfected cells ($p =$

0.005), but no change was observed in the luciferase activity of Mut-*Syap1* ($p = 0.793$) (Figure 5B), indicating that miR-590-3p can specifically bind to *Syap1*.

miR-590-3p down-regulates mRNA levels of Syap1, TGF-β, and Smad3

The results of RT-qPCR (Figure 6) illustrated that compared with the normal mice, the expression of miR-590-3p was notably increased, while the mRNA levels of *Syap1*, TGF-β, Smad3, and NF-κB p65 were much lower, and the mRNA expression of TNF-α, IL-1β, and IL-6 was higher in the lung tissues of modeled mice. Compared with the blank control, the expression of miR-590-3p ($p < 0.0001$), TNF-α ($p < 0.0001$), IL-1β ($p = 0.015$), and IL-6 ($p < 0.0001$) was remarkably higher, while the mRNA expression of *Syap1* ($p = 0.001$), TGF-β ($p = 0.033$), Smad3 ($p = 0.002$), and NF-κB p65 ($p = 0.015$) was significantly lower in the lung tissues of mice treated with miR-590-3p agomir, and the results were opposite in the mice treated with miR-590-3p antagomir: the expression of miR-590-3p ($p = 0.024$), TNF-α ($p < 0.0001$), IL-1β ($p = 0.002$), and IL-6 ($p = 0.002$) was reduced, while the mRNA expression of *Syap1* ($p = 0.042$), TGF-β ($p < 0.0001$), Smad3 ($p = 0.036$), and NF-κB p65 ($p = 0.002$) was enhanced.

Compared with the NC and the blank control, there was no significant difference in miR-590-3p expression of the lung tissues of mice injected with *Syap1* ($p > 0.05$), while mRNA expression of *Syap1* ($p = 0.013$), TGF-β ($p = 0.002$), Smad3 ($p = 0.006$), and NF-κB p65 ($p = 0.002$) was markedly elevated, and that of TNF-α ($p < 0.0001$), IL-1β ($p = 0.002$), and IL-6 ($p = 0.003$) was decreased. The level of miR-590-3p ($p < 0.0001$) was significantly higher in the lung tissues of mice treated with both miR-590-3p agomir and *Syap1* in comparison to the blank control or NC, while the mRNA expression of *Syap1* ($p = 0.001$) was lower, and there was no significant difference in others ($p > 0.05$).

miR-590-3p inactivates TGF-β/Smad signaling pathway by down-regulating Syap1

Western blot analysis (Figure 7) showed that as compared with the normal mice, the protein expression of *Syap1*, TGF-β, Smad3, and NF-κB p65 was notably decreased, while that of TNF-α, IL-1β, and IL-6 was increased in the lung tissues of modeled mice ($p < 0.05$). Compared with the blank control or the NC, the protein expression of *Syap1* ($p < 0.0001$), TGF-β ($p < 0.0001$), Smad3 ($p < 0.0001$), and NF-κB p65 ($p = 0.0002$) was decreased, but that of TNF-α ($p < 0.0001$), IL-1β ($p < 0.0001$), and IL-6 ($p < 0.0001$) was obviously increased in the lung tissues of mice injected with miR-590-3p agomir, while the protein expression of *Syap1* ($p = 0.001$), TGF-β ($p < 0.0001$), Smad3 ($p < 0.0001$), and NF-κB p65 ($p < 0.0001$) was increased, but that of TNF-α ($p < 0.0001$), IL-1β ($p < 0.0001$), and IL-6 ($p < 0.0001$) was reduced in the mice treated with miR-590-3p antagomir. *Syap1* ($p = 0.0002$), TGF-β ($p < 0.0001$), Smad3 ($p < 0.0001$), and NF-κB p65 ($p < 0.0001$) expression in lung tissues of mice treated with *Syap1* was increased while the expression of TNF-α ($p < 0.0001$), IL-1β ($p < 0.0001$), and IL-6 ($p < 0.0001$) was significantly lower. The protein expression of *Syap1* was remarkably lower in the lung tissues of mice treated with both miR-590-3p agomir and *Syap1* ($p < 0.0001$) when compared with the blank control or the NC, and there was no

significant difference in others ($p > 0.05$). In sum, these results indicated that miR-590-3p can inhibit TGF-β/Smad signaling pathway by downregulating *Syap1*.

Western blot (Supplementary Figure 2) showed that LDN-212845 (BMP inhibitor) did not affect the TGF-β/Smad signaling pathway, while LDN-193189 could affect the TGF-β/Smad signaling pathway. After LDN-212845 was used to inhibit the BMP signaling pathway, it was found that LDN-212845 did not affect the TGF signal pathway reflected by protein expression of TGF-β and Smad1/3/5/8. This result reflected that the inhibition of LDN-193189 on BMP signaling pathway did not affect the effect of LDN-193189 on TGF-β/Smad signaling pathway.

Discussion

Sepsis is a serious inflammatory disease caused by infection, which could result in multiple organ failure (Essandoh et al., 2015). Since up to 30% of patients in the intensive care unit will experience severe symptoms, finding a suitable intervention target is essential to prevent their development into severe sepsis and septic shock and further lead to organ failure or even death (Ludwig and Hummon, 2017). Therefore, this study explored miR-590-3p related mechanisms in sepsis progression. The results demonstrated that miR-590-3p can mediate the TGF-β/Smad signaling pathway via inhibiting the expression of *Syap1* to induce sepsis inflammation and aggravate organ dysfunction.

Initially, we found that miR-590-3p expression was upregulated, while *Syap1* expression was downregulated and TGF-β/Smad signaling pathway was inactivated in modeled mice. In allied findings, Salem et al. reported that miR-590-3p was highly expressed in epithelial ovarian cancer and promoted its development through the FOXA2-VCAN pathway (Salem et al., 2018). It is established that miRNAs are small non-coding RNAs with only 21-25 nucleotides, which are widely expressed in eukaryotic cells and play important roles in many diseases (Liu et al., 2015). Some miRNAs have been implicated in sepsis related pathology. For instance, Wang et al. showed that inhibition of miR-21-3p alleviates sepsis-associated cardiac dysfunction by negatively regulating SH3 domain-containing protein 2 (Wang et al., 2016). Liu et al. suggested that downregulation of miR-199a can suppress the excessive inflammatory responses and alleviate sepsis-induced acute lung injury through upregulation of SIRT1 (Liu et al., 2018). In this study, miR-590-3p was also found to be upregulated and play a role in lungs and livers of sepsis-affected mice.

TGF-β signaling pathway is a multifunctional cytokine contains numerous family members, which can mediate the normal development of tissues and organs and effectively suppress the immune system (Kloss et al., 2018). For instance, Cao and co-workers reported that miR-145 regulates sepsis-induced lung injury through TGFBR2 signaling (Cao et al., 2019). Zhang et al. indicated that SUMO protease SENP1 promotes sepsis via activating the TGFBR2 signaling (Zhang et al., 2019). Another study has shown that TGF-β, as one of the anti-inflammatory genes, could promote the anti-inflammatory ability of the body in combating sepsis (Molinaro et al., 2019). Here, we found that downregulated miR-590-3p could activate the TGF-β/Smad signaling pathway by upregulating *Syap1*, which ameliorated sepsis inflammation and

organ dysfunction. In agreement, a previous report found that TGF-β pathway activation could attenuate sepsis-induced weakness in rats, and SMAD3 was also associated with sepsis (Jude et al., 2019). Reduced levels of TNF-α, IL-1β, and IFN-γ are indication of less severe inflammation (Souza et al., 2012), and IL-6 also serves as a pro-inflammatory cytokine, while IL-10 is an anti-inflammatory cytokine (Rong et al., 2018). The increased levels of ALT and AST can reflect liver injury (van Beek et al., 2013). Based on our findings, downregulated miR-590-3p suppressed severe sepsis inflammation and organ dysfunction as evidenced by reduced expression TNF-α, IL-1β, IL-6, IFN-γ, AST, and ALT but upregulated expression of IL-10. In a related finding, a recent study indicated that miR-590-3p can alleviate acute kidney injury via the inhibition of TNF receptor-6 in sepsis-affected mice (Ma et al., 2019). Zohreh et al. have previously noted that miR-590-3p could inhibit cell survival and promote apoptosis of breast cancer cells by targeting sirtuin-1 and deacetylation of p53 (Abdolvahabi et al., 2019). Likewise, we found that miR-590-3p could promote the apoptotic rate of lung and liver cells in sepsis-affected mice in our study.

Our findings not only highlighted the importance of miR-590-3p in sepsis-affected mice, but also provided clues for underlying clinical applications. In view of the fact that only a limited number of CLP mouse models were successfully conducted in this study, we will expand the sample size to form more robust conclusions and verify the role of miR-590-3p in inflammation and organ dysfunction in sepsis.

Conclusion

In conclusion, our investigations offered a new insight into the specific mechanism of miR-590-3p in sepsis modeled mice. In this study, we identified a mechanism where the suppression of miR-590-3p can upregulate the expression of *Syap1* to activate the TGF-β/Smad signaling pathway, so as to inhibit inflammatory response and reduce organ dysfunction in sepsis. Our findings suggest that with further investigation, miR-590-3p may emerge as a potentially innovative therapeutic and diagnostic target for sepsis-related inflammation and organ dysfunction.

Declarations

DATA AVAILABILITY STATEMENT

The datasets generated and/or analysed during the current study are available from the corresponding author on reasonable request.

ETHICS STATEMENT

The animal experiments were performed in strict accordance with the recommendations in the ‘Guide to the Management and Use of Laboratory Animals’ issued by the National Institutes of Health. The protocol for animal experiments was approved by the Institutional Animal Care and Use Committee of The First Affiliated Hospital of Fujian Medical University.

AUTHOR CONTRIBUTIONS

YML, YJH, and XFH wrote the main manuscript text, ZHL collected the data, and YML prepared all figures. All authors reviewed the manuscript.

FUNDING

None.

ACKNOWLEDGMENTS

We would like express sincere appreciation to the reviewers for critical comments regarding this article.

CONFLICTS OF INTERESTS

The authors confirm that there are no conflicts of interest.

References

Abdolvahabi, Z., Nourbakhsh, M., Hosseinkhani, S., Hesari, Z., Alipour, M., Jafarzadeh, M., et al. (2019). MicroRNA-590-3P suppresses cell survival and triggers breast cancer cell apoptosis via targeting sirtuin-1 and deacetylation of p53. *J Cell Biochem.* 120, 9356-9368. doi: 10.1002/jcb.28211

Azeh, I., Gerber, J., Wellmer, A., Wellhausen, M., Koenig, B., Eiffert, H., et al. (2002). Protein synthesis inhibiting clindamycin improves outcome in a mouse model of Staphylococcus aureus sepsis compared with the cell wall active ceftriaxone. *Crit Care Med.* 30, 1560-1564. doi: 10.1097/00003246-200207000-00027

Benz, F., Roy, S., Trautwein, C., Roderburg, C. and Luedde, T. (2016). Circulating MicroRNAs as Biomarkers for Sepsis. *Int J Mol Sci.* 17, doi: 10.3390/ijms17010078

Cao, X., Zhang, C., Zhang, X., Chen, Y. and Zhang, H. (2019). MiR-145 negatively regulates TGFBR2 signaling responsible for sepsis-induced acute lung injury. *Biomed Pharmacother.* 111, 852-858. doi: 10.1016/j.biopha.2018.12.138

Chang, Y. C., Yu, Y. L., Wang, N. and Xu, Y. H. (2001). [Cloning and characterization of syap1, a down regulated gene in human hepatocellular carcinoma]. *Shi Yan Sheng Wu Xue Bao.* 34, 319-322.

de Pablo, R., Monserrat, J., Reyes, E., Diaz, D., Rodriguez-Zapata, M., la Hera, A., et al. (2012). Sepsis-induced acute respiratory distress syndrome with fatal outcome is associated to increased serum transforming growth factor beta-1 levels. *Eur J Intern Med.* 23, 358-362. doi: 10.1016/j.ejim.2011.10.001

Essandoh, K., Yang, L., Wang, X., Huang, W., Qin, D., Hao, J., et al. (2015). Blockade of exosome generation with GW4869 dampens the sepsis-induced inflammation and cardiac dysfunction. *Biochim Biophys Acta.* 1852, 2362-2371. doi: 10.1016/j.bbadis.2015.08.010

Fernando, S. M., Rochwerg, B. and Seely, A. J. E. (2018). Clinical implications of the Third International Consensus Definitions for Sepsis and Septic Shock (Sepsis-3). *CMAJ.* 190, E1058-E1059. doi: 10.1503/cmaj.170149

Gotts, J. E. and Matthay, M. A. (2016). Sepsis: pathophysiology and clinical management. *BMJ.* 353, i1585. doi: 10.1136/bmj.i1585

Jude, B., Tissier, F., Dubourg, A., Droguet, M., Castel, T., Leon, K., et al. (2020). TGF-beta Pathway Inhibition Protectsthe Diaphragm From Sepsis-Induced Wasting and Weakness in Rat. *Shock.* 2020 Jun;53(6):772-778. doi: 10.1097/SHK.0000000000001393

Kingsley, S. M. K. and Bhat, B. V. (2017). Role of microRNAs in sepsis. *Inflamm Res.* 66, 553-569. doi: 10.1007/s00011-017-1031-9

Kloss, C. C., Lee, J., Zhang, A., Chen, F., Melenhorst, J. J., Lacey, S. F., et al. (2018). Dominant-Negative TGF-beta Receptor Enhances PSMA-Targeted Human CAR T Cell Proliferation And Augments Prostate Cancer Eradication. *Mol Ther.* 26, 1855-1866. doi: 10.1016/j.ymthe.2018.05.003

Kohler, J., Maletzki, C., Koczan, D., Frank, M., Trepesch, C., Revenko, A. S., et al. (2020). The contact system proteases play disparate roles in streptococcal sepsis. *Haematologica.* 2020 May;105(5):1424-1435. doi:

10.3324/haematol.2019.223545.

Liu, J., Shi, K., Chen, M., Xu, L., Hong, J., Hu, B., et al. (2015). Elevated miR-155 expression induces immunosuppression via CD39(+) regulatory T-cells in sepsis patient. *Int J Infect Dis.* 40, 135-141. doi: 10.1016/j.ijid.2015.09.016

Liu, Y., Guan, H., Zhang, J. L., Zheng, Z., Wang, H. T., Tao, K., et al. (2018). Acute downregulation of miR-199a attenuates sepsis-induced acute lung injury by targeting SIRT1. *Am J Physiol Cell Physiol.* 314, C449-C455. doi: 10.1152/ajpcell.00173.2017

Ludwig, K. R. and Hummon, A. B. (2017). Mass spectrometry for the discovery of biomarkers of sepsis. *Mol Biosyst.* 13, 648-664. doi: 10.1039/c6mb00656f

Ma, J., Li, Y. T., Zhang, S. X., Fu, S. Z. and Ye, X. Z. (2019). MiR-590-3p Attenuates Acute Kidney Injury by Inhibiting Tumor Necrosis Factor Receptor-Associated Factor 6 in Septic Mice. *Inflammation.* 42, 637-649. doi: 10.1007/s10753-018-0921-5

Molinaro, R., Pasto, A., Corbo, C., Taraballi, F., Giordano, F., Martinez, J. O., et al. (2019). Macrophage-derived nanovesicles exert intrinsic anti-inflammatory properties and prolong survival in sepsis through a direct interaction with macrophages. *Nanoscale.* 11, 13576-13586. doi: 10.1039/c9nr04253a

Patel, A., Joseph, J., Periasamy, H. and Mokale, S. (2018). Azithromycin in Combination with Ceftriaxone Reduces Systemic Inflammation and Provides Survival Benefit in a Murine Model of Polymicrobial Sepsis. *Antimicrob Agents Chemother.* 62, doi: 10.1128/AAC.00752-18

Rong, Y. D., Bian, A. L., Hu, H. Y., Ma, Y. and Zhou, X. Z. (2018). Study on relationship between elderly sarcopenia and inflammatory cytokine IL-6, anti-inflammatory cytokine IL-10. *BMC Geriatr.* 18, 308. doi: 10.1186/s12877-018-1007-9

Rupaimoole, R. and Slack, F. J. (2017). MicroRNA therapeutics: towards a new era for the management of cancer and other diseases. *Nat Rev Drug Discov.* 16, 203-222. doi: 10.1038/nrd.2016.246

Salem, M., O'Brien, J. A., Bernaudo, S., Shawer, H., Ye, G., Brkic, J., et al. (2018). miR-590-3p Promotes Ovarian Cancer Growth and Metastasis via a Novel FOXA2-Versican Pathway. *Cancer Res.* 78, 4175-4190. doi: 10.1158/0008-5472.CAN-17-3014

Schmitt, D., Funk, N., Blum, R., Asan, E., Andersen, L., Rulicke, T., et al. (2016). Initial characterization of a Syap1 knock-out mouse and distribution of Syap1 in mouse brain and cultured motoneurons. *Histochem Cell Biol.* 146, 489-512. doi: 10.1007/s00418-016-1457-0

Souza, C. O., Peracoli, M. T., Weel, I. C., Bannwart, C. F., Romao, M., Nakaira-Takahagi, E., et al. (2012). Hepatoprotective and anti-inflammatory effects of silibinin on experimental preeclampsia induced by L-NAME in rats. *Life Sci.* 91, 159-165. doi: 10.1016/j.lfs.2012.06.036

van Beek, J. H., de Moor, M. H., de Geus, E. J., Lubke, G. H., Vink, J. M., Willemsen, G., et al. (2013). The genetic architecture of liver enzyme levels: GGT, ALT and AST. *Behav Genet.* 43, 329-339. doi: 10.1007/s10519-013-9593-y

van der Poll, T., van de Veerdonk, F. L., Scicluna, B. P. and Netea, M. G. (2017). The immunopathology of sepsis and potential therapeutic targets. *Nat Rev Immunol.* 17, 407-420. doi: 10.1038/nri.2017.36

Wang, H., Bei, Y., Shen, S., Huang, P., Shi, J., Zhang, J., et al. (2016). miR-21-3p controls sepsis-associated cardiac dysfunction via regulating SORBS2. *J Mol Cell Cardiol.* 94, 43-53. doi: 10.1016/j.yjmcc.2016.03.014

Wang, H. F., Li, Y., Wang, Y. Q., Li, H. J. and Dou, L. (2019). MicroRNA-494-3p alleviates inflammatory response in sepsis by targeting TLR6. *Eur Rev Med Pharmacol Sci.* 23, 2971-2977. doi: 10.26355/eurrev_201904_17578

Wrighton, K. H., Lin, X. and Feng, X. H. (2009). Phospho-control of TGF-beta superfamily signaling. *Cell Res.* 19, 8-20. doi: 10.1038/cr.2008.327

Yuan, F. H., Chen, Y. L., Zhao, Y., Liu, Z. M., Nan, C. C., Zheng, B. L., et al. (2019). microRNA-30a inhibits the liver cell proliferation and promotes cell apoptosis through the JAK/STAT signaling pathway by targeting SOCS-1 in rats with sepsis. *J Cell Physiol.* 234, 17839-17853. doi: 10.1002/jcp.28410

Zhang, C., Li, J., Qiu, X., Chen, Y. and Zhang, X. (2019). SUMO protease SENP1 acts as a ceRNA for TGFBR2 and thus activates TGFBR2/Smad signaling responsible for LPS-induced sepsis. *Biomed Pharmacother.* 112, 108620. doi: 10.1016/j.biopha.2019.108620

Figures

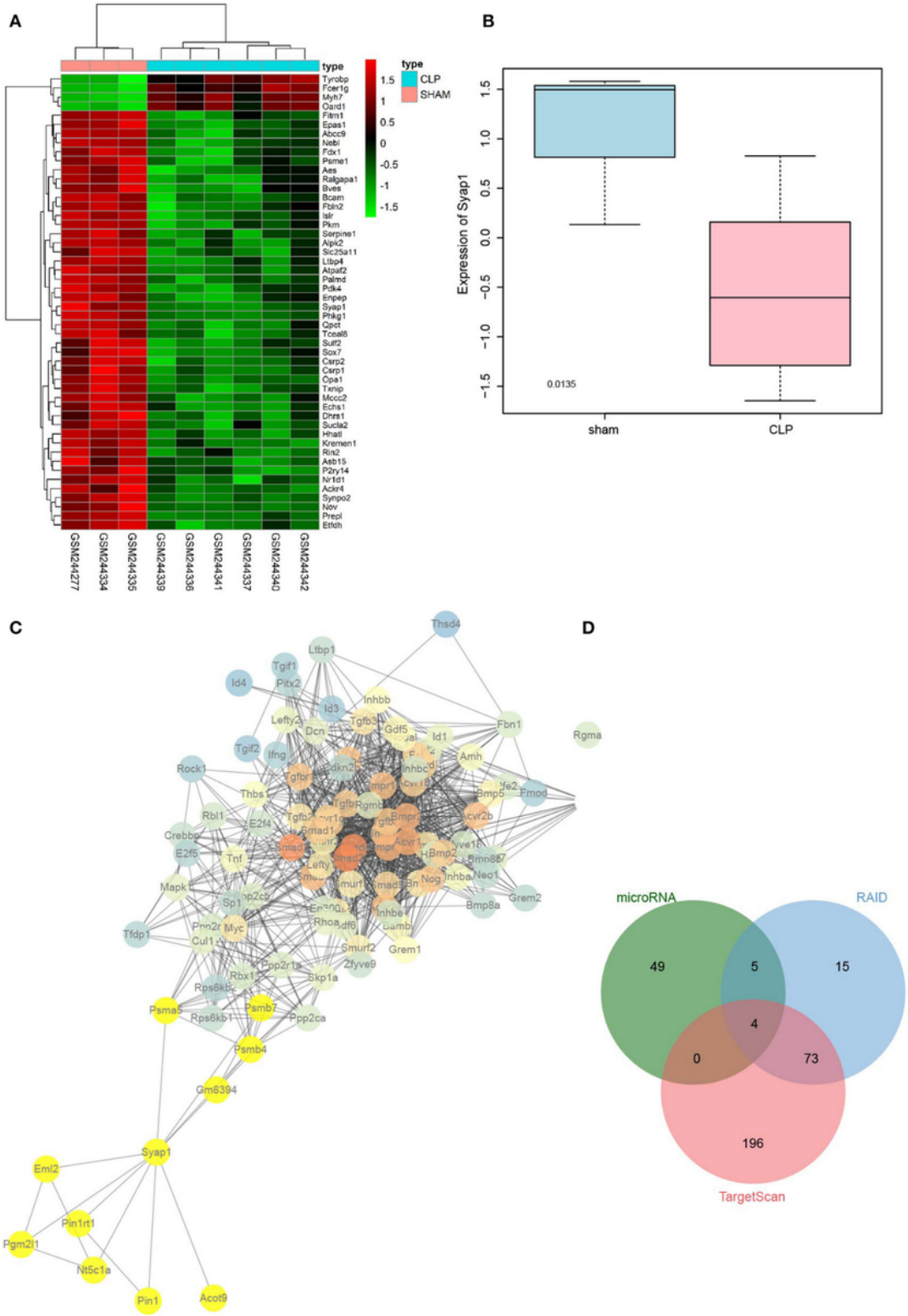

Figure 1

Results of microarray analysis. A, Heat map of differentially expressed genes in the gene-expression dataset GSE9667-GPL339 (the redder square indicates higher expression, while the greener square indicates an opposite trend); B, Syap1 expression in the gene dataset GSE9967-GPL339 (blue box indicates the expression of the normal sample, and red box indicates the expression of the sepsis sample); C, Syap1 related genes and TGF-β/Smad signaling pathway analyzed by PPI (red circle indicates higher core degree; yellow circle represents directly related gene of Syap1); D, The Venn map of the upstream miRs of Syap1 obtained by microRNA, RAID2.0, and TargetScan databases, and the intersecting miRs were miR-291a-3P, miR-340-5p, miR-384-5p, and miR-590-3p.

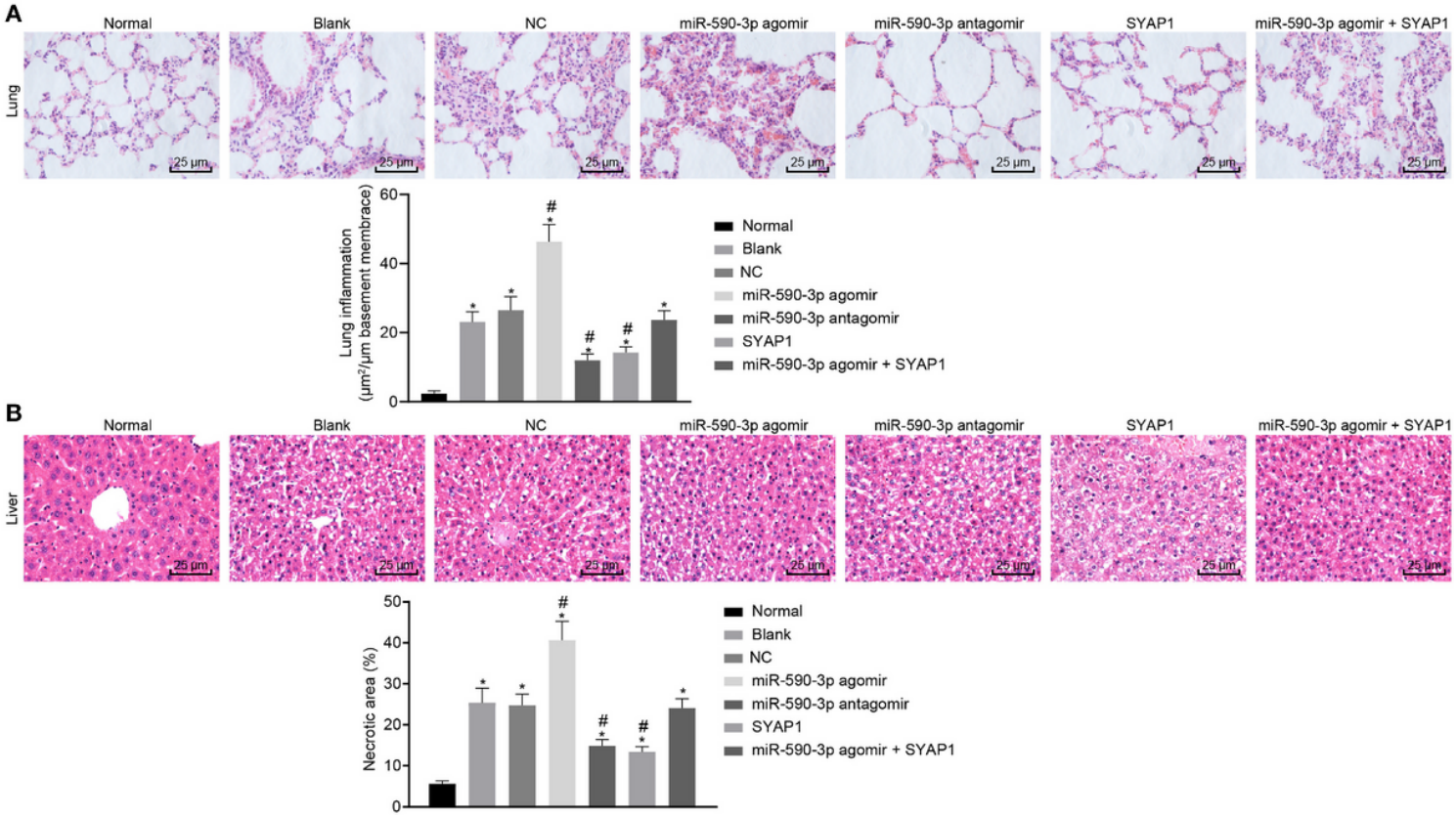

Figure 2

HE staining of lung and liver tissues of various mice groups with different treatments. Eight healthy mice were selected as the normal control (health mice without any treatment). And 40 successfully modeled mice were selected and every 8 mice were injected via tail vein with miR-590-3p agomir (10 mg/kg, 200 μL), miR-590-3p antagomir (10 mg/kg, 200 μL miR-590-3p interference plasmid), Syap1 interference lentivirus (specific interference with Syap1 lentivirus), miR-590-3p agomir combined with Syap1 interference lentivirus (10 mg/kg, 200 μL miR-590-3p agomir + Syap1), and the corresponding negative control (NC, CLP mouse injected via tail vein with equal volume sterile PBS). And 8 successfully modeled mice were selected as the blank control (The CLP mouse model without any treatment). A, HE staining of lung tissues of mice in each group (× 400). B, HE staining of liver tissues of mice in each group (× 400). * $p < 0.05$ vs. normal mice. The data were measurement data, and presented as mean ± standard deviation. One-way ANOVA was used for the data comparison between groups, with Tukey's post hoc test, n = 8.

Normal, healthy mice without any treatment; Blank, modeled mice without any treatment; NC, modeled mice treated with sterile PBS.

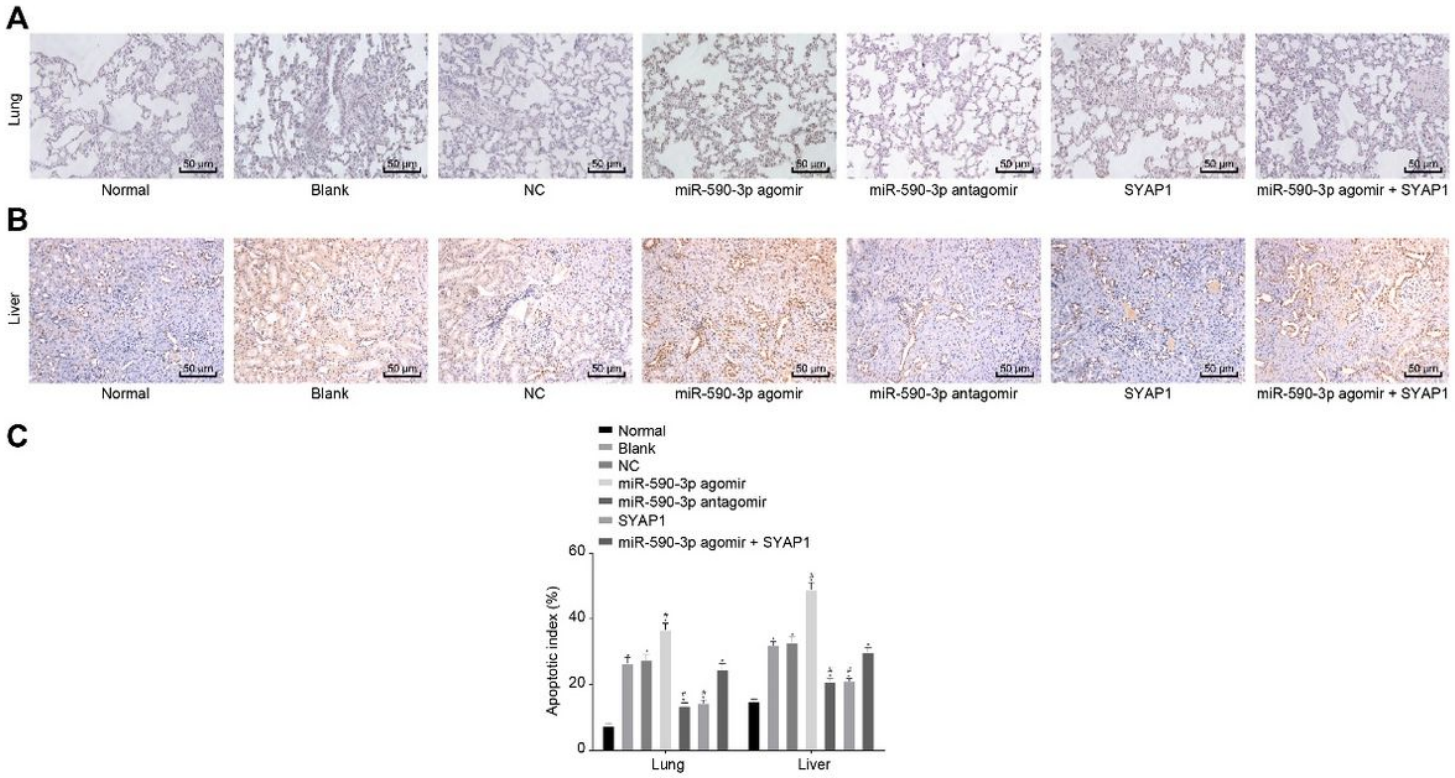

Figure 3

TUNEL staining results of lung and liver tissues of various mice groups with different treatments. A, TUNEL staining of lung tissues (× 400); B, TUNEL staining of liver tissues (× 400); C, the apoptotic rate of lung and liver cells; * $p < 0.05$ vs. normal mice; # $p < 0.05$ vs. blank control and NC. Normal, healthy mice without any treatment; Blank, modeled mice without any treatment; NC, modeled mice treated with sterile PBS. The data were measurement data, and presented as mean ± standard deviation. One-way ANOVA was used for the data comparison between groups, with Tukey's post hoc test, n = 8. The experiments were repeated for 3 times.

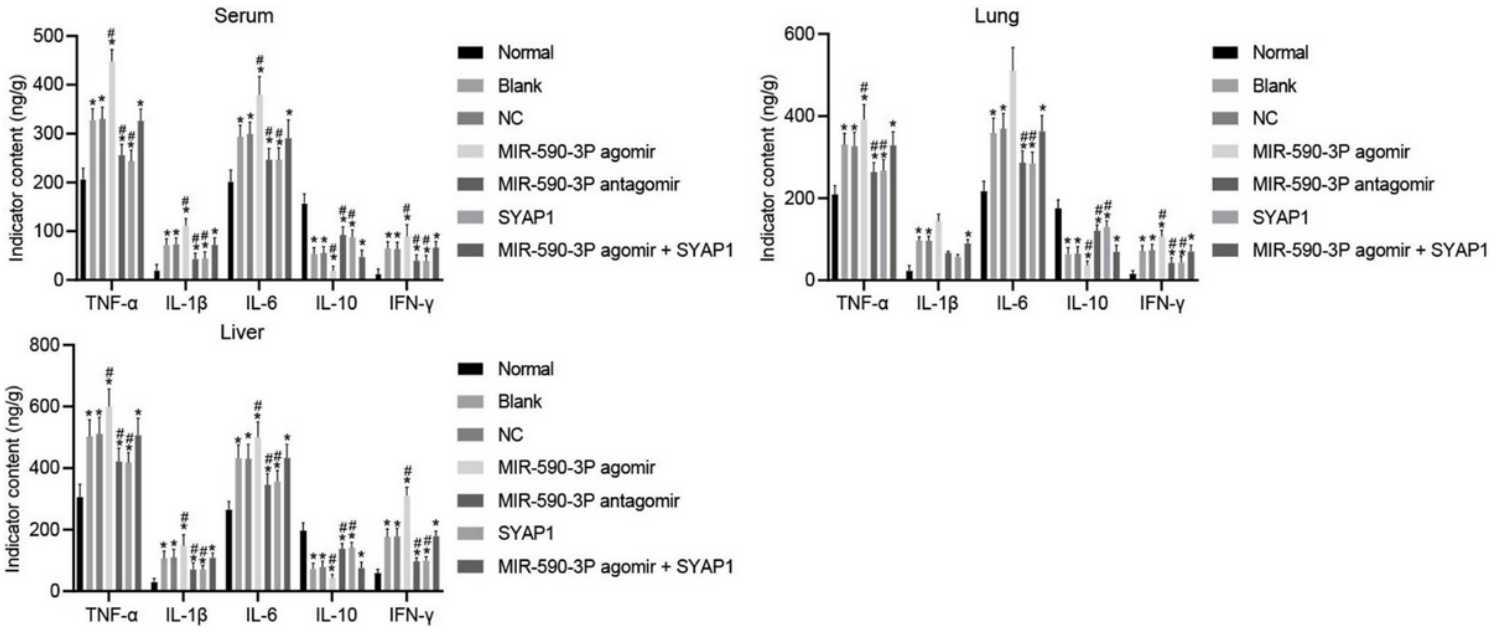

Figure 4

Expression of TNF-α, IL-1β, IL-6, IL-10, and IFN-γ in mouse serum, lungs, and livers. * p < 0.05 vs. the normal mice; # p < 0.05 vs. the blank control or NC. Normal, healthy mice without any treatment; Blank, modeled mice without any treatment; NC, modeled mice treated with sterile PBS. Tissues in the common liver or lung of different groups of mice were separated, measured with vernier calipers, and weighed. The tissues were ground and the levels of cytokines were determined. The data were measurement data, and presented as mean ± standard deviation. One-way ANOVA was used for the data comparison among multiple groups, with Tukey's post hoc test, n = 8. The experiments were repeated for 3 times.

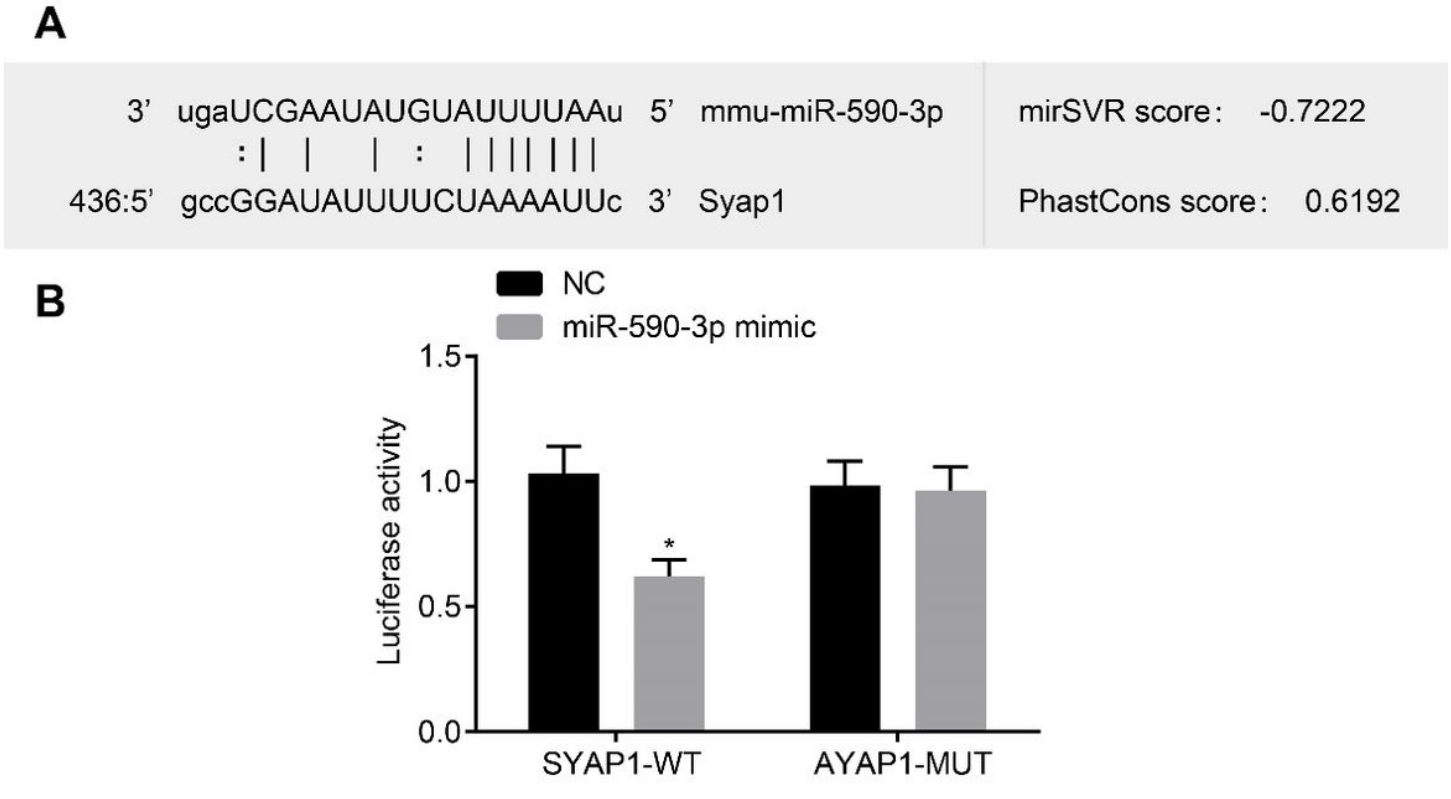

Figure 5

miR-590-3p could target Syap1. The correctly sequenced luciferase reporter plasmids WT and mutant (MUT) were co-transfected with the miR-590-3p into the HEK-293T cells respectively. A, Bin ding site map of Syap1 and miR-590-3p in microRNA database; B, luciferase activity of the WT-Syap1 and MUT-Syap1 in cells treated with miR-590-3p mimic and NC. * $p < 0.05$ vs. NC. The data were measurement data, expressed as mean ± standard deviation. Unpaired t test was used for the data comparison between two groups, and the experiment was repeated for three times.

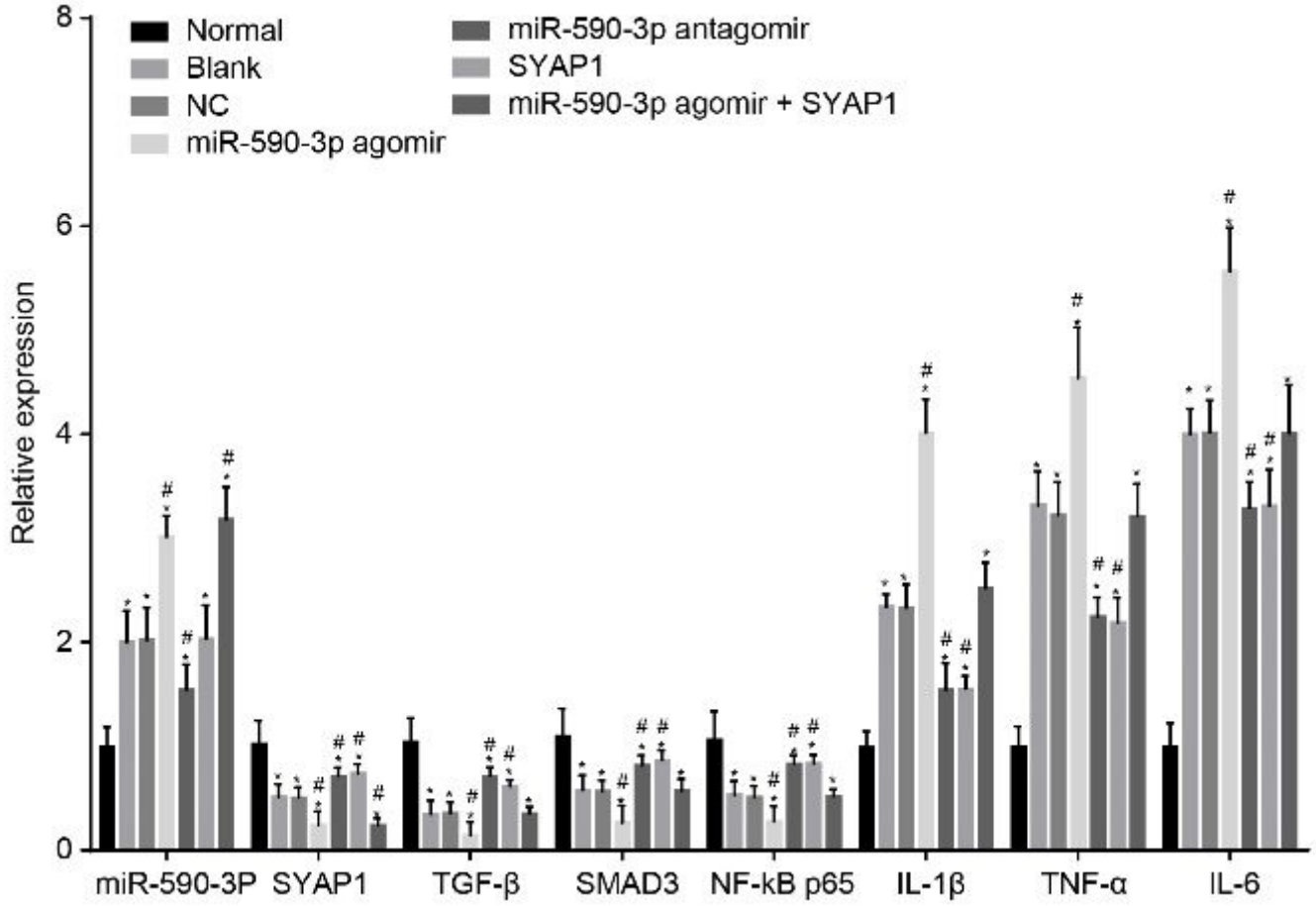

Figure 6

Upregulated miR-590-3p inhibits the inflammatory response in lung tissues of mice. * $p < 0.05$ vs. normal mice; # $p < 0.05$ vs. blank control or NC. Normal, healthy mice without any treatment; Blank, modeled mice without any treatment; NC, modeled mice treated with sterile PBS. The data were measurement data, and expressed as mean ± standard deviation. One-way ANOVA was used for comparison among multiple groups, with Tukey's post hoc test, n = 8. The experiments were repeated for 3 times.

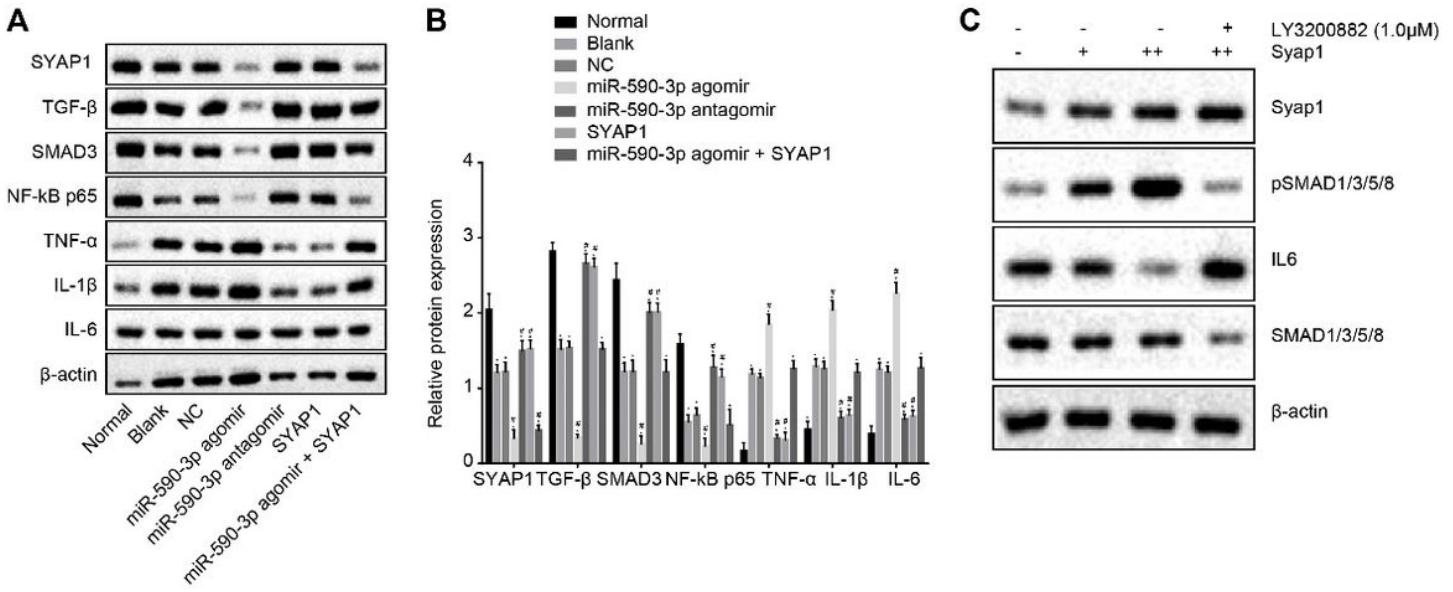

Figure 7

miR-590-3p blocks TGF-β/Smad signaling pathway by repressing Syap1. A, Protein expression of related genes in lung tissues of mice by Western blot analysis. B, Corresponding quantitation histogram of A. C, Smad phosphorylation and expression of inflammatory factors in lung epithelial cell A549 transfected with different contents of Syap1 plasmid and TGF-β/Smad signaling pathway inhibitor LDN-193189 determined by Western blot. Normal, healthy mice without any treatment; Blank, modeled mice without any treatment; NC, modeled mice treated with sterile PBS. * $p < 0.05$ vs. normal mice; # $p < 0.05$ vs. blank control and NC. The data were measurement data, and presented as mean ± standard deviation. One-way ANOVA was used for the data comparison among multiple groups, with Tukey's post hoc test, n = 8. The experiments were repeated for 3 times.

Supplementary Files

This is a list of supplementary files associated with this preprint. Click to download.

- SUPPLEMENTARYFIGURE1.jpeg
- SUPPLEMENTARYFIGURE2.jpeg